

## Supporting Information

# Controllable Sulfur Vacancy Engineering and Lean-Liquid System for Enhanced Solar-Driven Hydrogen Evolution on Metal Sulfide Photocatalysts

Lingling Ding<sup>a</sup>, Kun Li<sup>a</sup>, Kun Chang<sup>a\*</sup>

<sup>a</sup> Centre for Hydrogenergy, College of Materials Science and Technology, Nanjing University of Aeronautics and Astronautics, Nanjing 210016, PR China

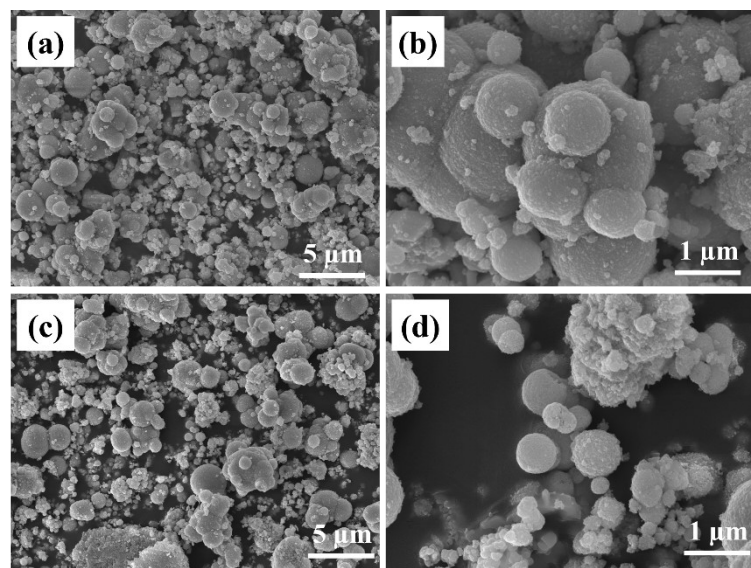


Figure S1. SEM images of CIZS (a-b) before and (c-d) after vulcanization.

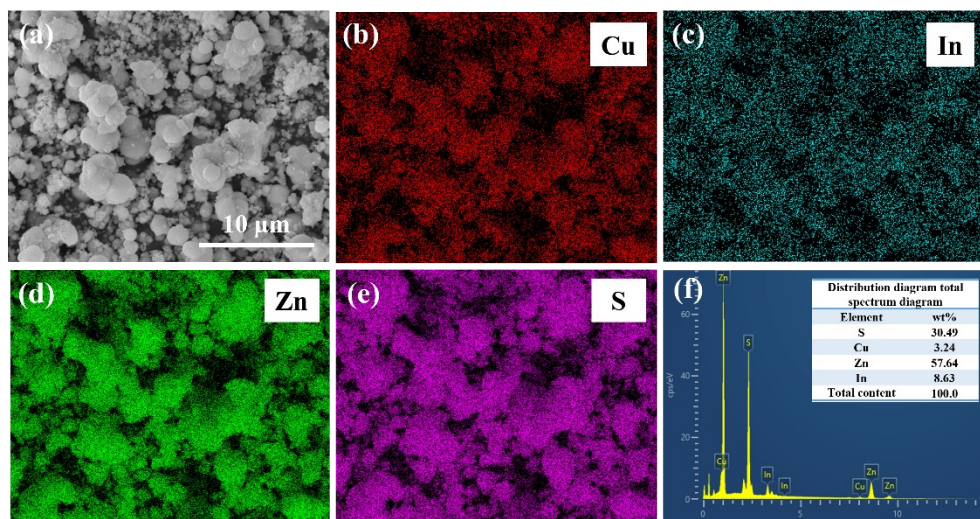


Figure S2. EDX elemental mapping images of CIZS.

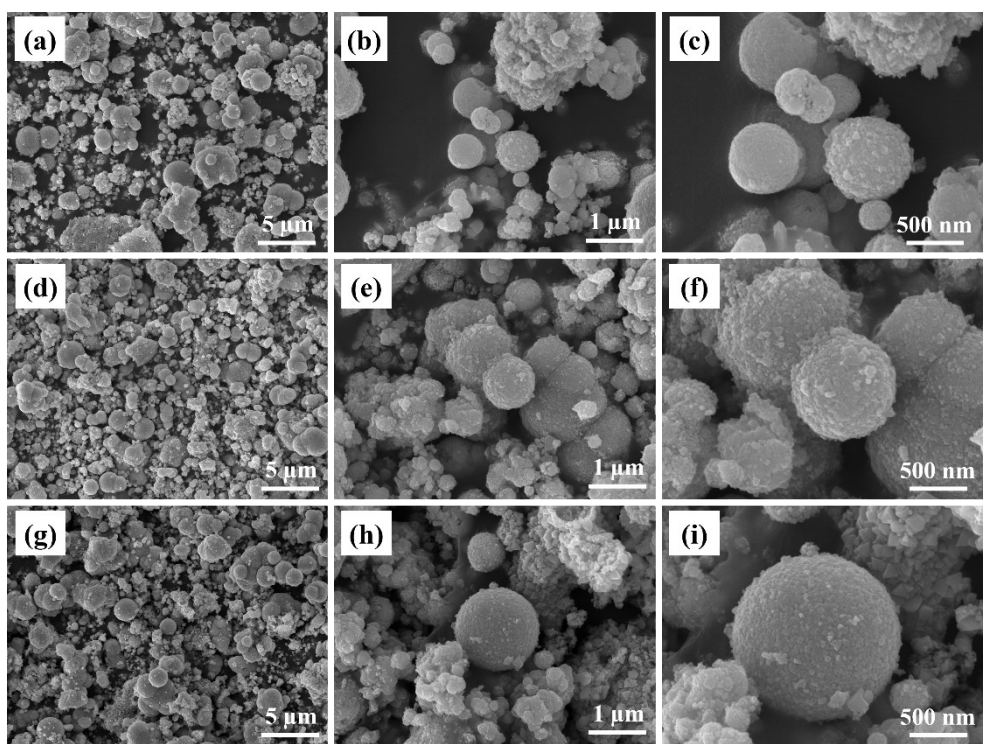


Figure S3. SEM images of (a-c) 0S<sub>v</sub>/CIZS, (d-f) 10S<sub>v</sub>/CIZS, (g-i) 30S<sub>v</sub>/CIZS.

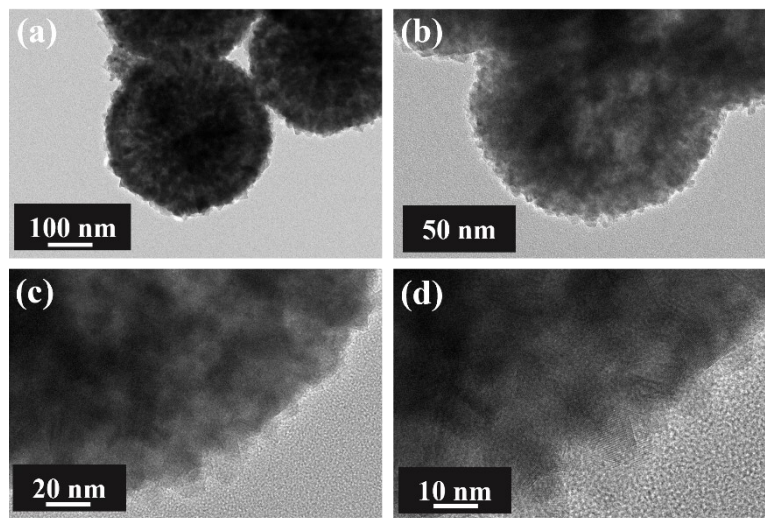


Figure S4. TEM images of 10 S<sub>v</sub>/CIZS.

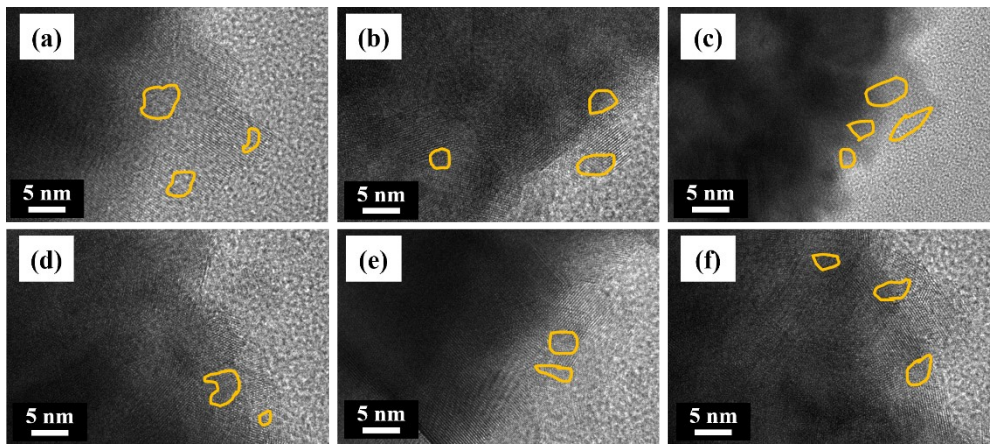


Figure S5. HRTEM images of 10 S<sub>v</sub>/CIZS.

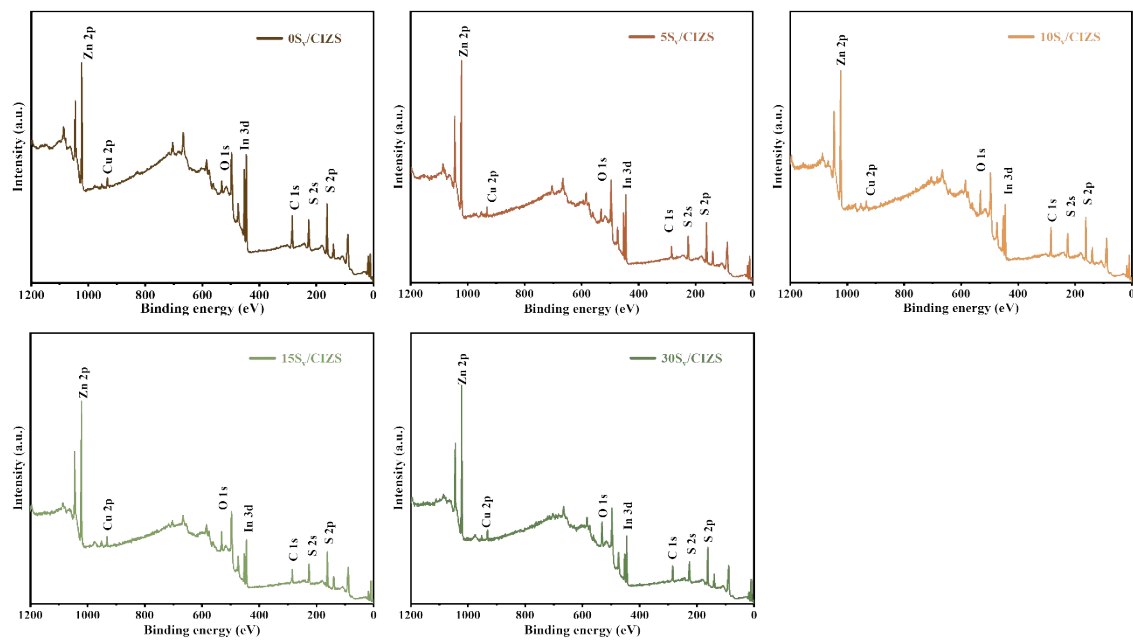


Figure S6. XPS spectra of  $0\text{-}30\text{S}_v/\text{CIZS}$ .

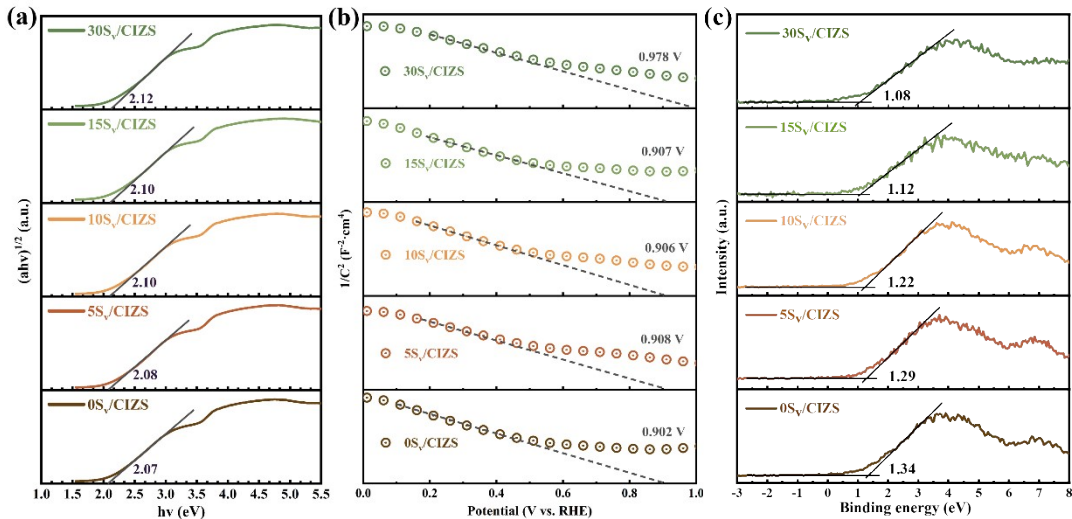


Figure S7. (a) Corresponding Tauc plots, (b) Mott-schottky curves, (c) VB-XPS spectra of 0-30S<sub>v</sub>/CIZS.

Based on the UV-VIS diffuse reflection spectrum, the semiconductor band gap is calculated using the Tauc formula. As depicted in Figure S7a, it can be observed that the band gaps of 0-30S<sub>v</sub>/CIZS are 2.07, 2.08, 2.10, 2.11, and 2.12 eV respectively. The Mott-Schottky test is a commonly used analytical method for electrochemical testing of photocatalytic semiconductor materials. Hence, to clarify the semiconductor properties of S<sub>v</sub>/CIZS, a Mott-Schottky test was carried out on the S<sub>v</sub>/CIZS photocathode at 2000 Hz, as presented in Figure S7b. The slope of the measured  $1/C^2$  versus potential is negative, which is in line with the negative slope characteristic of a typical p-type semiconductor. The flat-band potential of S<sub>v</sub>/CIZS is approximately 0.91 V relative to the reversible hydrogen electrode. For the 30S<sub>v</sub>/CIZS sample, due to the overly long PCVD treatment time, it induces the generation of unsaturated coordination sulfur atoms. This leads to an increase in the charge density within the Cu-S, In-S, and Zn-S bonds, and the electron density of the S element also increases, ultimately raising the flat band potential of the semiconductor to 0.98 V. Figure S7c displays the VB-XPS spectra of the S<sub>v</sub>/CIZS samples. According to the conversion formula, the valence bands of the samples are 1.45, 1.40, 1.33, 1.23, and 1.19 V respectively.

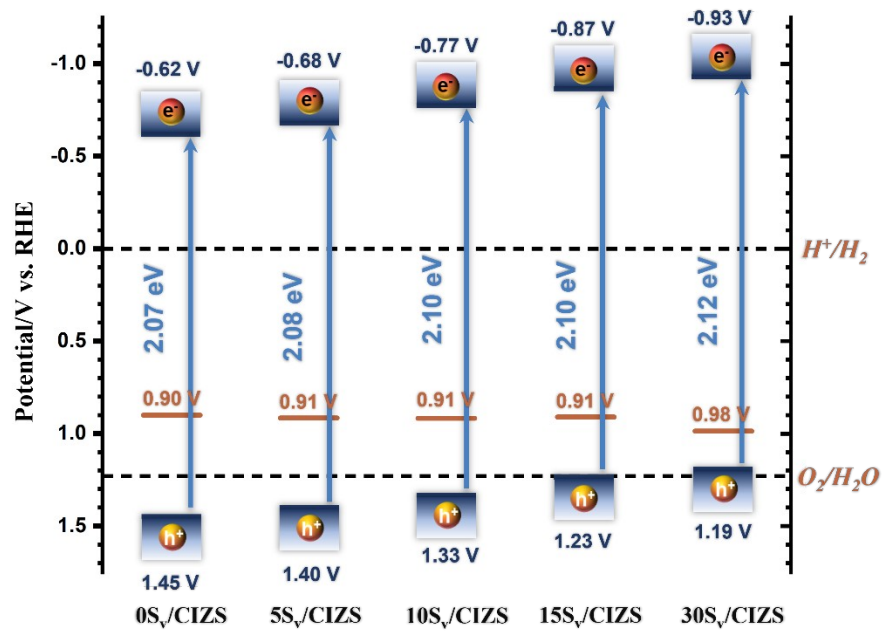


Figure S8. Band structures of 0-30S<sub>v</sub>/CIZS.

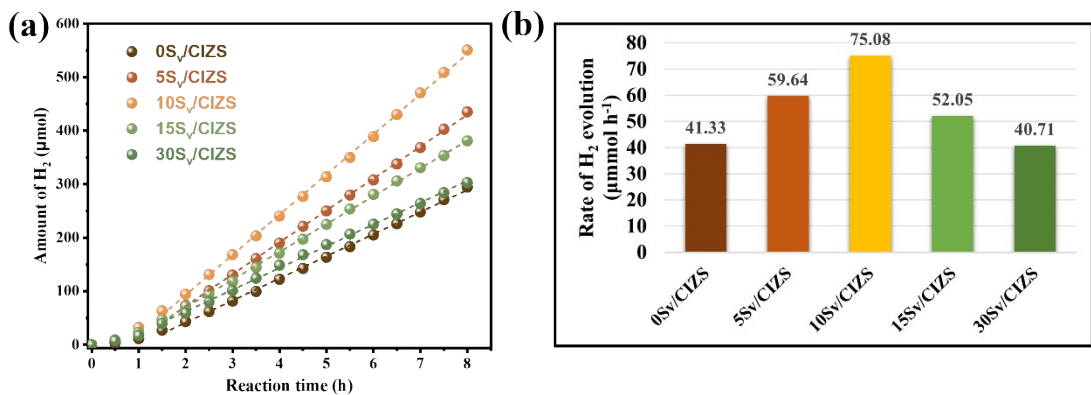


Figure S9. Photocatalytic HER under visible-light ( $\lambda > 420$  nm) irradiation of 0-30S<sub>v</sub>/CIZS.

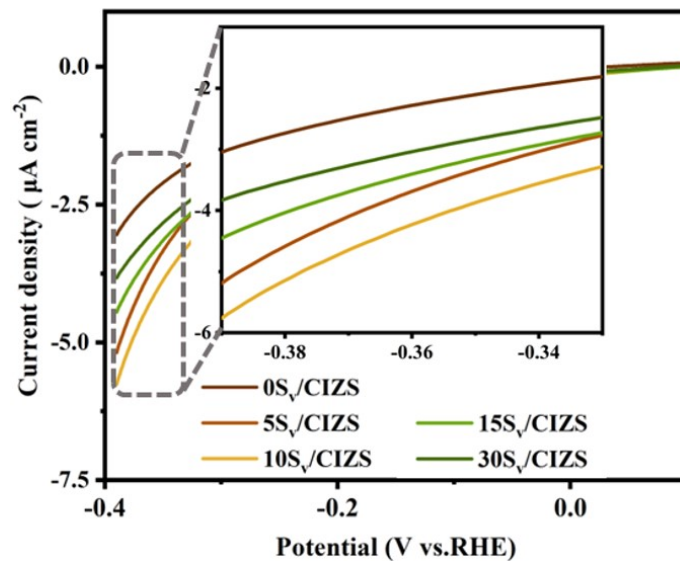


Figure S10. Photocurrent density vs potential curves of 0- $30S_v/\text{CIZS}$ .

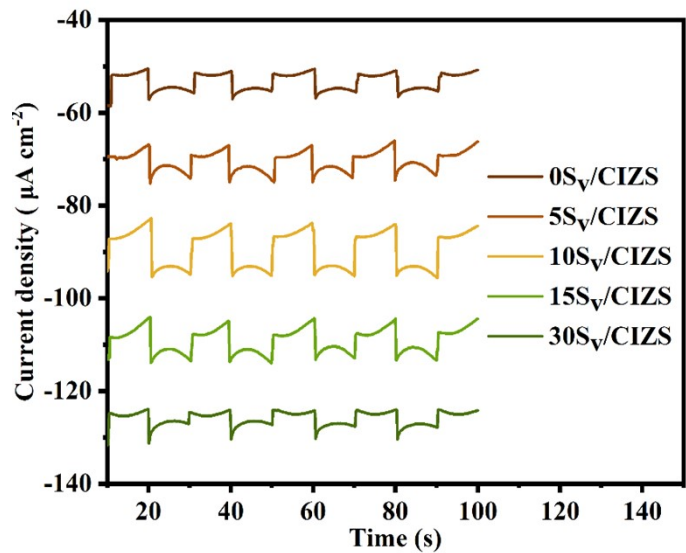


Figure S11. Chopped light time-dependent photocurrent of 0-30 $S_v$ /CIZS.

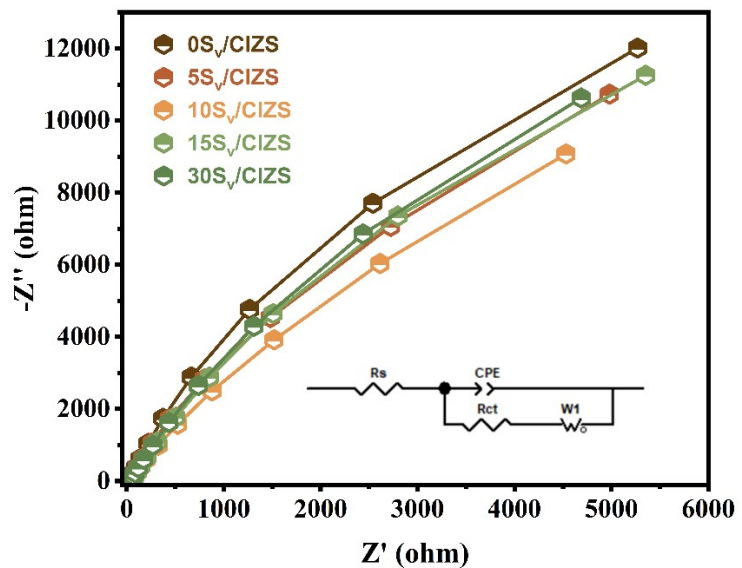


Figure S12. Electrochemical impedance spectroscopy Nyquist diagram of 0-  
 $30S_v/CIZS$ .

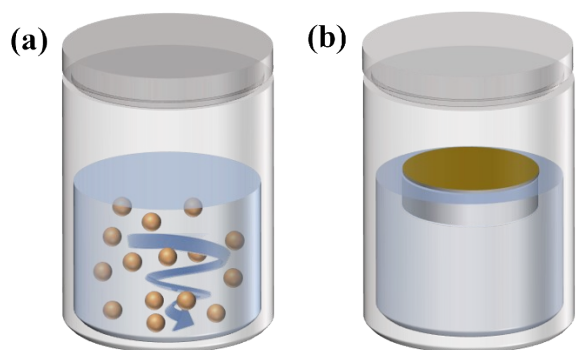


Figure S13. (a) Liquid-phase suspension system, (b) Lean-liquid system

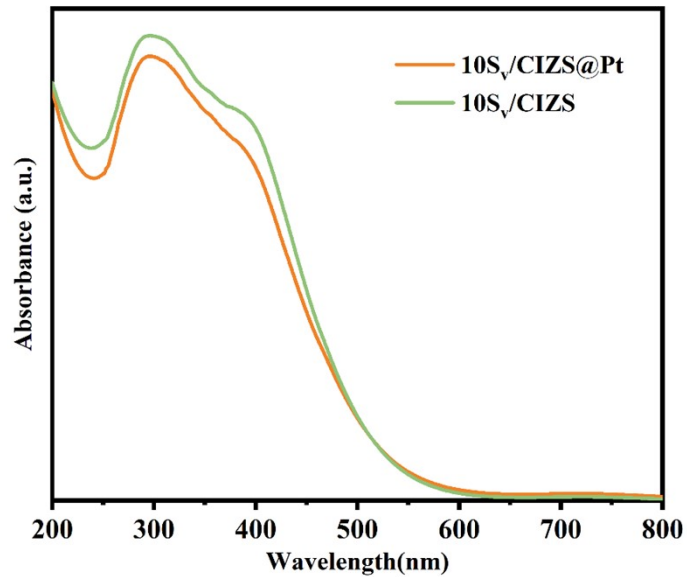


Figure S14. UV-Vis DRS spectra of  $10S_v/\text{CIZS}$  and  $10S_v/\text{CIZS}@\text{Pt}$ .

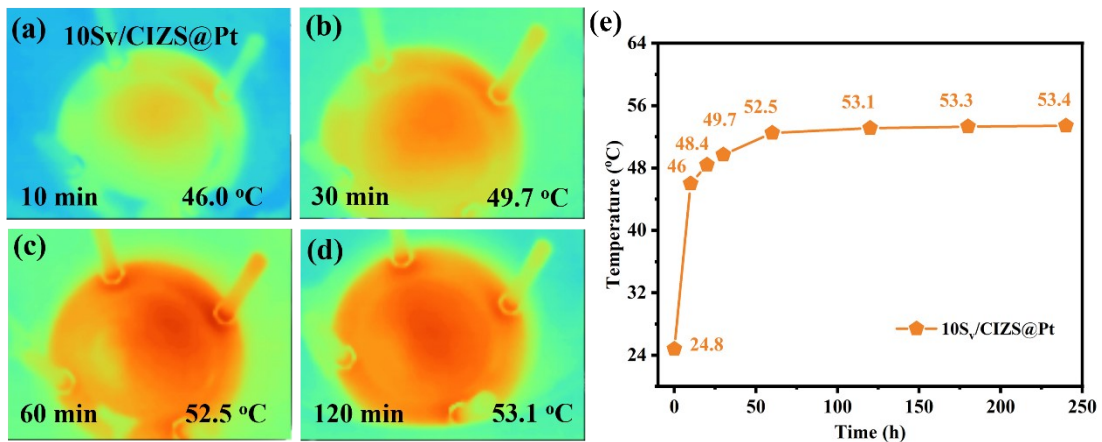


Figure S15. (a-d) Infrared thermograms of typical reaction systems using  $10S_v/CIZS@Pt$  at various illumination times by visible-light ( $\lambda > 420$  nm) irradiation; (e) Correlation of illumination time and temperature.

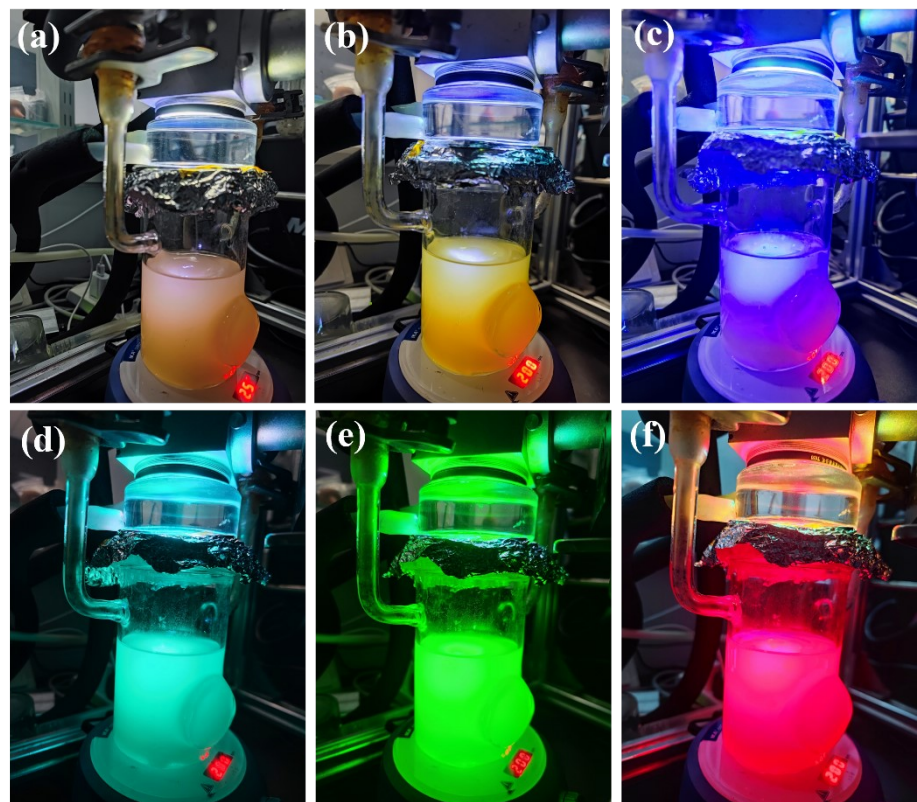


Figure S16. Test images of  $10S_v/CIZS@Ru$  photocatalyzed HER under different wavelength irradiation.

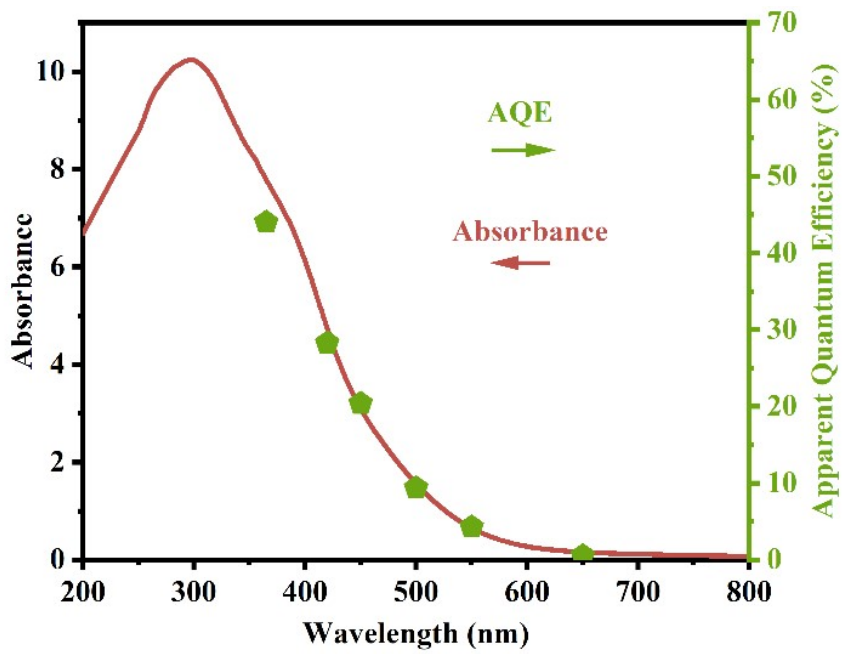


Figure S17. AQY of 10S<sub>v</sub>/CIZS@Ru with monochromatic light.

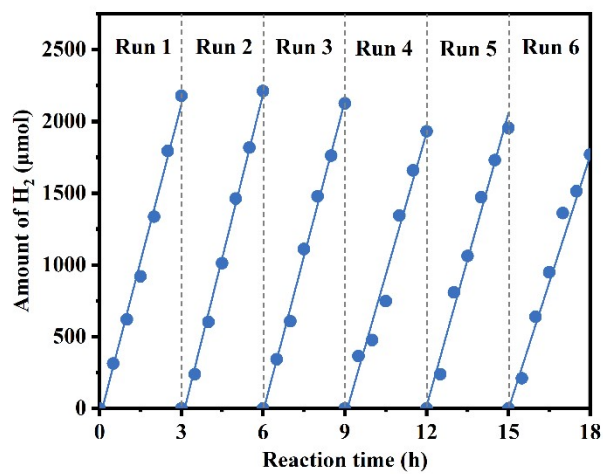


Figure S18. Cyclic test of photocatalytic hydrogen evolution performance of 10S<sub>v</sub>/CIZS@Ru semiconductor ( $\lambda > 420$  nm).

Table S1. Surface compositions and chemical state of sulfur species over as-prepared photocatalysts

| Sample                 | BE (eV) | Cont. (%) | BE (eV) | Cont. (%) | R    |
|------------------------|---------|-----------|---------|-----------|------|
| 0S <sub>v</sub> /CIZS  | 163.51  | 29.56     | 162.33  | 70.44     | 0.42 |
| 5S <sub>v</sub> /CIZS  | 163.38  | 31.91     | 162.11  | 68.09     | 0.47 |
| 10S <sub>v</sub> /CIZS | 163.34  | 33.59     | 162.06  | 66.41     | 0.51 |
| 15S <sub>v</sub> /CIZS | 163.28  | 33.22     | 162.04  | 66.78     | 0.50 |
| 30S <sub>v</sub> /CIZS | 163.10  | 38.81     | 161.98  | 65.19     | 0.59 |

Table S2 The AQY of 10S<sub>v</sub>/CIZS@Ru for photocatalytic H<sub>2</sub> production.

| <b>λ (nm)</b> | <b>H<sub>2</sub> evolution<br/>(μmol·h<sup>-1</sup>)</b> | <b>I (mW·cm<sup>-2</sup>)</b> | <b>AQE (%)</b> |
|---------------|--|-------------------------------|----------------|
| 365           | 23.65  | 9.77                          | 44.01          |
| 420           | 18.50  | 10.34                         | 28.27          |
| 450           | 31.75  | 22.96                         | 20.39          |
| 500           | 12.63  | 17.47                         | 9.39           |
| 550           | 7.26   | 19.58                         | 4.25           |
| 650           | 0.84   | 15.92                         | 0.53           |

Table S3. Kinetic parameters of the charge carrier decay in 10S<sub>v</sub>/CIZS and 10S<sub>v</sub>/CIZS@Ru

| Catalyst                  | τ <sub>1</sub> (ns) | A <sub>1</sub> | τ <sub>2</sub> (ns) | A <sub>2</sub> | τ <sub>avg</sub> (ns) |
|---------------------------|---------------------|----------------|---------------------|----------------|-----------------------|
| 0S <sub>v</sub> /CIZS     | 0.6763              | 43.52          | 5.236               | 56.48          | 3.5836                |
| 10S <sub>v</sub> /CIZS    | 0.6182              | 34.61          | 5.7042              | 65.39          | 3.9441                |
| 10S <sub>v</sub> /CIZS@Ru | 0.7177              | 25.33          | 8.0350              | 74.67          | 6.1816                |

Table S4 Comparison of the photocatalytic H<sub>2</sub> production performances in this study

with literature results.

| <b>Photocatalysts</b>   | <b>Light source</b>                         | <b>Sacrificial agent</b>                                      | <b>H<sub>2</sub> evolution (μmol g<sup>-1</sup> h<sup>-1</sup>)</b> | <b>Year</b>  | <b>Ref.</b> |
|---|---|---|---|--------------|-------------|
| <b>Photocatalytic</b>   |   |   |   |              |             |
| CIZS-rGO<br>(Solvothermal method)   | 800 W Xe-Hg lamp                            | Na <sub>2</sub> S/Na <sub>2</sub> SO <sub>3</sub><br>solution | 3800  | 2013         | [1]         |
| CIZS QDs<br>(Hydrothermal method)   | 300 W Xe lamp<br>(λ > 420 nm)               | Na <sub>2</sub> S/Na <sub>2</sub> SO <sub>3</sub><br>solution | 456.4   | 2018         | [2]         |
| CIZS QDs<br>(One-pot aqueous method)  | Xe lamp<br>(λ = 400-780 nm).                | 0.2MAA<br>(pH=5.0)  | 14400   | 2018         | [3]         |
| CZIS nanobelts<br>(Colloidal method)  | 300 W Xe lamp                               | Na <sub>2</sub> S/Na <sub>2</sub> SO <sub>3</sub><br>solution | 3350  | 2020         | [4]         |
| CIZS@Ru<br>(Gel-assisted method)  | Xe lamp<br>(λ > 420 nm)                     | Na <sub>2</sub> S/Na <sub>2</sub> SO <sub>3</sub><br>solution | 4860  | 2022         | [5]         |
| CIZS/MoS <sub>2</sub> /CDs<br>(Hydrothermal method)   | white LED light<br>(AM 1.5G)                | 0.2 M L-ascorbic<br>acid                                      | 3706  | 2022         | [6]         |
| NiS <sub>2</sub> /PVP/CIZS<br>(Hydrothermal method)   | 300 W Xenon lamp<br>(λ > 420 nm)            | Na <sub>2</sub> S/Na <sub>2</sub> SO <sub>3</sub><br>solution | 5369.4  | 2022         | [7]         |
| S <sub>v</sub> /CIZS@Ru<br>(Hydrothermal method)  | 300 W Xenon lamp<br>(λ > 420 nm)            | Na <sub>2</sub> S/Na <sub>2</sub> SO <sub>3</sub><br>solution | 13336.2   | This<br>work |             |
| <b>Photothermal-catalytic</b>   |   |   |   |              |             |
| CoP@ZnIn <sub>2</sub> S <sub>4</sub> @Co <sub>3</sub> O <sub>4</sub><br>(Solvothermal approach) | 300 W Xenon lamp<br>(λ > 400 nm)            | Triethanolamine<br>(71.2 °C)                                  | 4254  | 2021         | [8]         |
| Pt/ZnIn <sub>2</sub> S <sub>4</sub><br>(Hydrothermal method)                                    | 300 W Xe lamp<br>(200 mW cm <sup>-2</sup> ) | Triethanolamine<br>(~45 °C)                                   | 19400   | 2022         | [9]         |
| FeS <sub>2</sub> @ZIS<br>(Solvothermal method)  | 300 W Xe lamp<br>(AM 1.5G)                  | Triethanolamine<br>(41.9 °C)                                  | 5050  | 2023         | [10]        |
| CDs/Ni <sub>3</sub> P/ZIS<br>(Hydrothermal method)  | 300 W Xe lamp<br>(200 mW cm <sup>-2</sup> ) | Triethanolamine<br>(~50 °C)                                   | 1880.78   | 2024         | [11]        |
| Fe <sub>3</sub> O <sub>4</sub> @SiO <sub>2</sub> /ZIS<br>(Hydrothermal method)                  | 300 W Xe lamp<br>(AM 1.5G)                  | Triethanolamine<br>(72.5 °C)                                  | 1258.5  | 2024         | [12]        |
| FNS@ZIS   | 300 W Xe lamp                               | Na <sub>2</sub> S/Na <sub>2</sub> SO <sub>3</sub>             | 7700  | 2024         | [13]        |

|  |                                |   |       |           |
|--|--------------------------------|---|-------|-----------|
| (Solvothermal method)                            |                                | Solution (32.8 °C)  |       |           |
| CNS/ZIS<br>(Solvothermal method)                 | 300 W Xe lamp                  | Triethanolamin<br>(~60 °C)  | 17168 | 2024 [14] |
| S <sub>v</sub> /CIZS@Ru<br>(Hydrothermal method) | 300 W Xenon lamp<br>(λ>420 nm) | Na <sub>2</sub> S/Na <sub>2</sub> SO <sub>3</sub><br>solution (53.8 °C) | 13336 | This work |

## References (S)

- [1] X. Tang, Q. Tay, Z. Chen, Y. Chen, G.K.L. Goh, J. Xue, *J. Mater. Chem. A*, 2013, **1**, 6359-6365.
- [2] L. Tan, Y. Liu, B. Mao, B. Luo, G. Gong, Y. Hong, B. Chen, W. Shi, *Inorg. Chem. Front.*, 2018, **5**, 258-265.
- [3] X.Y. Liu, G. Zhang, H. Chen, H. Li, J. Jiang, Y.T. Long, Z. Ning, *Nano Res.*, 2018, **11**, 1379-1388.
- [4] L. Wu, Q. Wang, T.T. Zhuang, Y. Li, G. Zhang, G.Q. Liu, F.J. Fan, L. Shi, S.H. Yu, *Nat. Commun.*, 2020, **11**, 5194.
- [5] Z. Xie, W. Xu, F. Fang, K. Zhang, X. Yu, K. Chang, *Chem. Eng. J.*, 2022, **429**, 132364.
- [6] Q. Chen, Y. Liu, X. Gu, D. Li, D. Zhang, D. Zhang, H. Huang, B. Mao, Z. Kang, W. Shi, *Appl. Catal. B Environ.*, 2022, **301**, 120755.
- [7] T. Feng, Y. Cao, R. Gao, G. Su, H. Li, B. Dong, L. Cao, *Int. J. Hydrogen Energy* 2022, **47**, 9934-9945.
- [8] T. Zhang, F. Meng, M. Gao, W.L. Ong, K.G. Haw, T. Ding, G.W. Ho, S. Kawi, *EcoMat*, 2021, **3**, e12152.
- [9] X. Guo, J. Li, Y. Wang, Z. Rui, *Catal. Today*, 2022, **402**, 210-219.
- [10] K. Chen, Y. Shi, P. Shu, Z. Luo, W. Shi, F. Guo, *Chem. Eng. J.*, 2023, **454**, 140053.
- [11] J. Jia, X. Guo, Y. Tang, W. Zeng, H. Zeng, Z. Rui, *Int. J. Hydrogen Energy*, 2024, **28**, 122-130.
- [12] Y. Shi, Z. Chen, P. Hao, P. Shan, J. Lu, F. Guo, W. Shi, *J. Colloid Interf. Sci.*, 2024, **653**, 1339-1347.
- [13] S. Wang, D. Zhang, X. Pu, L. Zhang, D. Zhang, J. Jiang, *Small*, 2024, **20**, 2311504
- [14] H. Qin, W. Zhang, S. Zhao, Z. Yao, Q. Zheng, P. Zhang, S. Zhang, X. Xu, *Chem. Eng. J.*, 2024, **489**, 151213.